coatings

MDPI

Article

Measurement and Interpretation of the Effect of Electrical Sliding Speed on Contact Characteristics of On-Load Tap Changers

Xingzu Yang [1], Shuaibing Li [1,*], Yi Cui [2], Yongqiang Kang [1], Zongying Li [1], Hongwei Li [3] and Haiying Dong [1]

[1] School of New Energy and Power Engineering, Lanzhou Jiaotong University, Lanzhou 730070, China
[2] School of Information Technology and Electrical Engineering, The University of Queensland, Brisbane 4072, Australia
[3] School of Automation and Electrical Engineering, Lanzhou Jiaotong University, Lanzhou 730070, China
* Correspondence: shuaibingli@mail.lzjtu.cn

Abstract: This paper analyzes the effect of sliding speed on the electrical conductivity and friction properties of the contact pair of an on-load tap changer (OLTC). Reciprocating current-carrying tribological tests were carried out on a rod–plate–copper–tin–copper contact galvanic couple at different sliding speeds in air and insulating oil media. The results show that as the sliding speed increases from 24 mm/s to 119 mm/s, the average contact resistance in air increases from 0.2 Ω to 0.276 Ω, and the average contact resistance in insulating oil also increases from 0.2 Ω to 0.267 Ω. At 119 mm/s, the maximum contact resistance in insulating oil reaches 0.3 Ω. The micro-topography images obtained by scanning electron microscopy show that with the increase in sliding speed, the wear mechanisms in the air are mainly abrasive wear and adhesive wear, and the wear mechanisms in oil are mainly layered wear and erosion craters; high sliding speed and arcing promote contact surface fatigue and crack generation. X-ray photoelectron spectroscopy was used to analyze the surface. The copper oxide in the air and the cuprous sulfide in the insulating oil cause the surface film resistance, and the total contact resistance increases accordingly. In addition, the test shows that 119 mm/s in air and 95 mm/s in insulating oil are the speed thresholds. Below these speed thresholds, the increase in contact resistance is mainly caused by mechanical wear. Above these thresholds, the increase in contact resistance is mainly caused by arc erosion and chemical oxidation processes. Non-mechanical factors exacerbate the deterioration of the contact surface and become the main factor for the increase in contact resistance.

Keywords: arc erosion; contact couple; contact resistance; on-load tap changer; sliding speed; wear

check for updates

Citation: Yang, X.; Li, S.; Cui, Y.; Kang, Y.; Li, Z.; Li, H.; Dong, H. Measurement and Interpretation of the Effect of Electrical Sliding Speed on Contact Characteristics of On-Load Tap Changers. *Coatings* **2022**, *12*, 1436. https://doi.org/10.3390/coatings12101436

Academic Editor: Ana-Maria Lepadatu

Received: 23 August 2022
Accepted: 26 September 2022
Published: 29 September 2022

Publisher's Note: MDPI stays neutral with regard to jurisdictional claims in published maps and institutional affiliations.

Copyright: © 2022 by the authors. Licensee MDPI, Basel, Switzerland. This article is an open access article distributed under the terms and conditions of the Creative Commons Attribution (CC BY) license (https://creativecommons.org/licenses/by/4.0/).

1. Introduction

As one of the critical components in a power transformer, the on-load tap changer (OLTC) is responsible for regulating the output voltage of the power transformer at the desired level through a series of complicated mechanical operations. The operation condition of an OLTC has a significant impact on the reliability of the transformer. According to the latest survey, 45% of the transformer failures are induced by OLTCs [1], among which mechanical faults induced by switch contacts, drive springs and other components account for more than 70% of the total OLTC faults [2]. With the extensive use of OLTCs in high-voltage converter transformers, step-up transformers of renewable energy farms and distribution transformers, and the increasing demand for voltage and reactive power regulation of the grid, the fault rate of oil-immersed OLTCs, compared to other components, gradually increases year by year, which may impair the safe and stable operation of transformers. According to the internal reports of State Grid Corporation of China and China Southern Power Grid Corporation, the OLTC has had the most significant fault proportion among all transformers' critical components. The sliding and static contact pair of an OLTC may

experience excessive aging, ablation and other faults during its operation, which puts a heavy strain on the reliability of the OLTC. The electrical sliding speed is among the various parameters that influence the friction and wear behavior of a contact couple in an OLTC. Therefore, it is necessary to develop a proactive strategy to protect the OLTC from severe faults and ensure the safe and reliable operation of the power transformer.

1.1. Literature Survey and Gaps

Over the past several decades, some efforts have been put forward to assess the aging condition of OLTCs with a focus on two directions, i.e., fault detection and fault mechanism. The fault detection of OLTCs usually involves collecting various signals relevant to the operation condition of OLTCs, such as vibration signals, ultrasonic signals and electrical signals. These signals are further used for OLTC condition assessment using time and frequency domain methods or some artificial intelligence algorithms [3]. For example, L. Allard et al. [1] introduced a practical tool based on the vibroacoustic method for defect detection and fault diagnosis of OLTCs. It demonstrated that defects such as contact dislocation and contact wear could be successfully identified, which helps determine the maintenance schedule for an OLTC. Ma, Y. et al. [3] proposed a fault diagnosis method for the on-load tap changer based on the current and vibration signals of the drive motor, studied the feature extraction method of the multi-source monitoring signal of the on-load tap changer and proposed the continuity of the current signal of the drive motor. According to the characteristics of time, the sum of absolute values and the empirical mode decomposition energy of vibration signal of the switch body, a fault diagnosis method for an on-load tap changer integrated with abnormal detection is proposed by combining random forest and isolated forest algorithms. The tap changer sample data verify the accuracy and effectiveness of the proposed method for fault identification. J. Fan et al. [4] analyzed the vibration signal during the OLTC switching process based on the recursive quantitative analysis (RQA) method and applied phase space reconstruction and recursive graph theory to obtain the recursive graph of the vibration signal during the OLTC switching process. They then introduced recursive quantitative indicators such as recursion rate, laminarity and certainty, and their statistical distribution results describe the dynamic characteristics of OLTC vibration signals. The research results show that the distribution range of the RQA index of the defined vibration signal can more accurately judge the operation state of the OLTC.

Through both laboratory and on-site measurements, it has been proven that the sliding speed has a significant impact on the electrical properties of the contact couple. X. Zhang et al. [5] used the response surface classification research method to construct a friction map and wear map of $Ag/MoS_2/WS_2$ nanocomposites at different sliding speeds. It was found that lower sliding speeds lead to plow wear and higher sliding speeds cause oxidation delamination. A higher sliding speed is favorable for the formation of transfer film. The friction coefficient and wear rate are stable and low at a sliding speed of 1 m/s and a normal force of 0.25 N. The wear patterns at different sliding speeds predicted the wear mechanism, friction coefficient and wear rate of $Ag/MoS_2/WS_2$ nanocomposites. R. Namus et al. [6] studied the effect of reciprocating sliding speed on the friction corrosion properties of Ti_6Al_4V alloy under cathodic and open circuit potential in simulated body fluid. The results show that the sliding speed significantly influences the microstructure of the worn surface, thus affecting the wear rate. The wear rate at low sliding speed is one order of magnitude lower than that at high sliding speed. Synergistic and antagonistic behaviors are closely related to sliding speed. T. Chen et al. [7] studied the effect of rotational speed on current-carrying tribological properties using rolling friction and a wear tester. As the rotational speed increased from 240 r/min to 600 r/min, the total friction force during the steady state increased from 3.8 N to 7.6 N, and the contact resistance decreased from 0.52 Ω to 0.34 Ω. Scanning electron microscopy and optical microscopy showed that high rotational speed and current promote surface fatigue and cracks. X-ray photoelectron spectroscopy results show that more nascent metal is exposed on the rolled surface at

higher speeds, which is favorable for electrical contact and no arcing at high rotational speeds. X. Xie et al. [8] investigated the effect of the sliding speed on the electrical contact performance of AuAgCu/Au coating. They found that the friction pair's contact resistance and contact stability decreased with speed. Some scholars have also researched the contact resistance between the contact pairs. S. Noguchi et al. [9] used the low frequency alternating current method to measure the inter-turn contact resistance and coil strain by applying an external field of 1–3 T to a single flat coil and discussed the relationship between the inter-turn contact resistance and coil strain. It is concluded that the contact resistance is related to the electromagnetic force. Y. Fukuyama et al. [10] evaluated how the contact structure affects shrinkage resistance through nanofabricated physical simulation samples, while T. Cheng et al. [11] analyzed the mechanism of dynamic contact resistance measurement (DRM) test results by analyzing the chemical composition of the contact surface, the force exerted on the contact and the temperature at point a on the contact surface. S. Sudipta et al. [12] designed, developed and demonstrated a tabletop experimental setup for contact resistance and discussed measurements during indentation. Using a combination of the contact resistance measurement accessory and indentation, a model was proposed to explain the change in contact resistance during deformation. The above research lays a good foundation for further revealing the effects of the sliding speed on the deterioration of the contact couple.

Based on the literature survey, it is found that existing research mainly focuses on the wear characteristics and deterioration mechanism of contact couples in the air and water environment. Little has been reported on the contact couples of OLTCs in insulating oil. As the oil-immersed OLTC approaches the designed life, its contact surface's electrical and mechanical properties change due to multiple switching wear, which may result in a substantial increase in the arcing and other types of faults. Therefore, it is essential to understand the friction behavior and degradation mechanism of contact couples to ensure the reliable operation of OLTCs.

1.2. Summary of Contributions

To address the above limitations, this paper presents a comprehensive investigation of the effects of the electrical sliding speed on the contact characteristics of OLTCs. The major contributions are summarized as follows:

1. A practical friction and wear testing platform was established for simulating the OLTC's contact couples' movement with different speeds in air and insulting oil environments.
2. Micro-morphology analysis was also performed using SEM, revealing the wear characteristics of the contact surface of the OLTC.
3. The element analysis using EDS and XPS proposes possible mechanisms of the friction and wear behavior of OLTC contact couples at different sliding speeds.

Compared with the studies of S. Noguchi et al. [9] and Y. Fukuyama et al. [10], this research further explains the forces existing in the dual friction pair in contact and builds a physical model of the relevant forces. The physical and chemical characteristics of the contact surface are judged by means of SEM, EDS and XPS; then, combined with the change trend of contact resistance, the evolution mechanism of contact resistance in insulating oil and air medium under different sliding speeds is obtained. T. Chen et al. [7] studied the effect of rotational speed on the current-carrying tribological characteristics using a rolling tribometer. It was found that with the increase in rotational speed, the contact resistance decreased, and high rotational speed promoted the generation of surface fatigue. Due to the different structures of the current-carrying friction pairs, our research found that there is a critical value in the variation trend of contact resistance with speed, which does not show a single variation trend, and the surface deterioration mechanism at high rotational speed changes, except for the effect of surface fatigue. In addition, the deteriorating effect of the arc on the surface is gradually enhanced.

The findings of this research will help to understand whether the sliding speed of the contact couple has a significant impact on the deterioration of OLTCs. They also provide helpful insight for transformer manufacturers in selecting an appropriate sliding speed of the contact couple of the OLTCs and offer significant help for asset management departments in assessing aging conditions, determining redundant equipment and making informed decisions on the operation maintenance schedules of their transformer assets.

2. Experimental Setup

2.1. Friction and Wear Testing Platform

The experimental friction and wear testing platform is shown in Figure 1; it consists of four major modules, namely a high-voltage power source (i.e., a voltage regulation console and a step-up transformer), a voltage divider, a resistive load and associated data acquisition systems. A high voltage of 2 kV (RMS value) and 50 Hz is first generated by the power source, which is then applied to the contact coupled in series with a resistive load. The resistive load is a 50 Ω cement resistor. A two-channel oscilloscope (model TEK DPO3014, Produced by American Tektronix International Co., Ltd., Beaverton, OR, USA) is used to measure the voltage applied to the contact couple through a voltage divider (model FRC-50 kV, produced by Yangzhou Husu Electric Power Technology Co., Ltd., Yangzhou, Jiangsu, China) using Channel 1) and the voltage of the cement resistor (Channel 2). In this way, the current flowing through the contact couple is calculated, which is then used to determine the contact resistance of the couple.

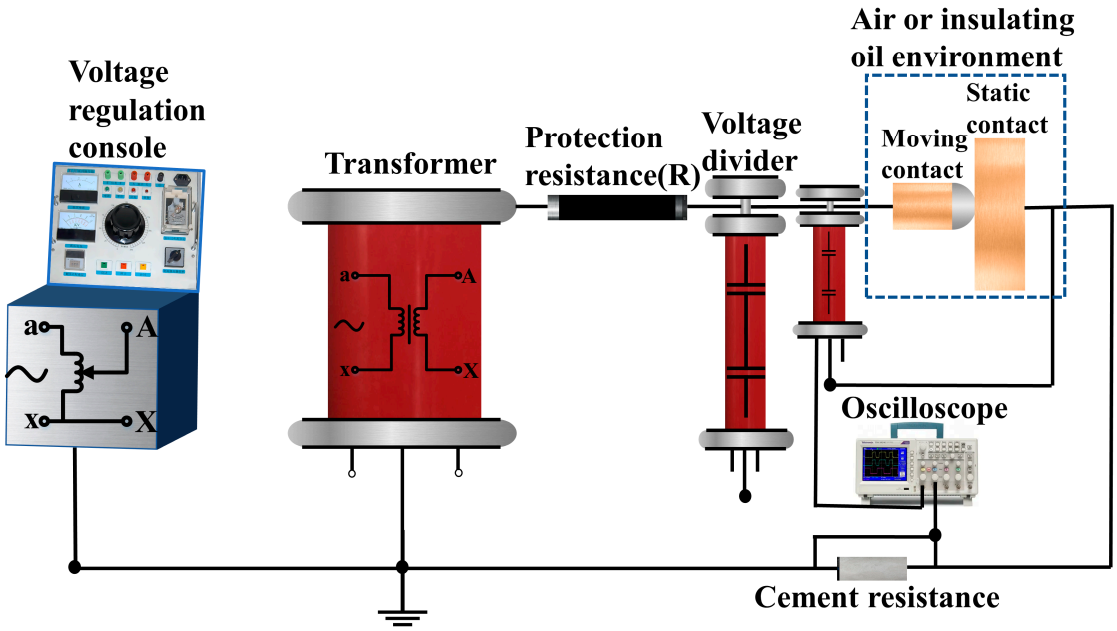

Figure 1. Schematic diagram of the friction and wear testing platform.

The material of the static contact is copper, and it has a rectangular shape with a length of 200 mm and a thickness of 20 mm. The moving contact has a cylinder shape with a diameter of 20 mm and a height of 35 mm. The material of the moving contact is also copper. However, the surface of the moving contact near the tip is coated with a silver coating film with 1.5 µm thickness. The weight percentage of different components of the moving contact is 40.01% copper, 24.65% tin, 14.85% carbon, 2% oxygen and other substances. Both static contact and moving contact are placed vertically, as shown in Figure 2. When the moving contact slides, it moves left and right horizontally without rolling. The contact pressure of the couple is less than the yield pressure of copper, and the contact couple is in elastic contact [13]. The contact couple is immersed in insulating oil to simulate the real-life operational condition of a transformer's OLTC.

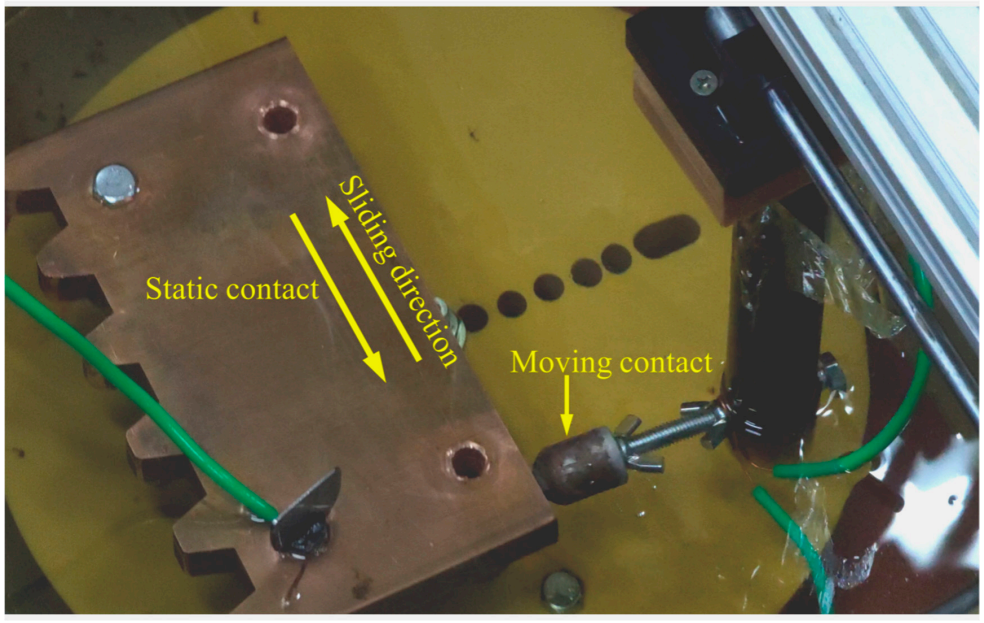

Figure 2. Image of real-life equipment for OLTC experimental test.

2.2. Testing Scenarios and Procedures

The friction and wear experiments were performed under two testing scenarios (i.e., air and insulting oil environment) using the established platform. For each testing scenario, five sliding speeds were selected: 25 mm/s, 50 mm/s, 75 mm/s, 100 mm/s and 125 mm/s. Due to the error of the motor driving the moving contact, the actual sliding speeds were 24 mm/s, 50 mm/s, 76 mm/s, 95 mm/s and 119 mm/s. Before each testing, the moving contact remained sliding on the static contact at 24 mm/s for 5 min without energizing the power supply. The sliding of the moving contact was controlled by a self-made position servo control system using a DC servo motor, H-bridge drive circuit and 80C51 single chip microcomputer. Detailed testing parameters are summarized in Table 1.

Table 1. Parameters of testing conditions.

Parameters	Set Value	Actual Value
Normal load Fn (N)	1.5	1.5
Sliding speed v (mm/s)	25/50/75/100/125	24/50/76/95/119
Diameter d (mm)	20	20
Sliding time t (min)	120	120
Electrical voltage U (kV)	2	2
Sliding distance D (mm)	200	200

A minimal difference in the mass was observed by measuring the mass of the static contact before and after the 5 min sliding. Then, the power supply was energized, and the friction and wear testing were continuously performed for 120 min at each sliding speed, during which the contact resistance is calculated every 20 min. After 120 min sliding, the moving contact was removed, and its tip was cut into a thin plate with a diameter of less than 10 mm. This plate was further used for SEM contact surface analysis using a Zeiss evo18 field emission scanning electron microscope (produced by Carl Zeiss AG, Oberkohen,, Germany). In addition, the elemental composition and chemical valence of the contact surface were also analyzed using a Bruker xflash 6130 energy dispersion X-ray spectrometer (produced by Bruker Technology Co., Ltd., Billerica, MA, USA) and Thermo Fisher k-alpha X-ray photoelectron spectrometer (produced by Thermo Fisher Scientific, Waltham, MA, USA), respectively. A new sample after each test replaced the moving contact. The static contact was polished by using sandpaper for the next round of testing.

3. Experimental Results and Discussion

3.1. Contact Resistance

3.1.1. Fluctuations of Contact Resistance over Time

Figure 3 shows the calculated contact resistance in both air and insulating oil at different sliding speeds. The contact resistance in both media has the same initial value of 0.2 Ω. There is an increasing trend in contact resistance when the sliding time is 20 min. Afterward, the contact resistance in the air becomes stable with minimal fluctuations. However, the contact resistance in the insulating oil shows significant variations, especially at the speed of 76 mm/s to 119 mm/s. Calculating the average contact resistance at 120 min for all five speeds shows that the contact resistance in the air increases by 37.9%, while it is 50% for the insulting oil compared with its initial value of 0.2 Ω. This implies that the conductivity of the contact surface is reduced after the substantial wear in the insulating oil.

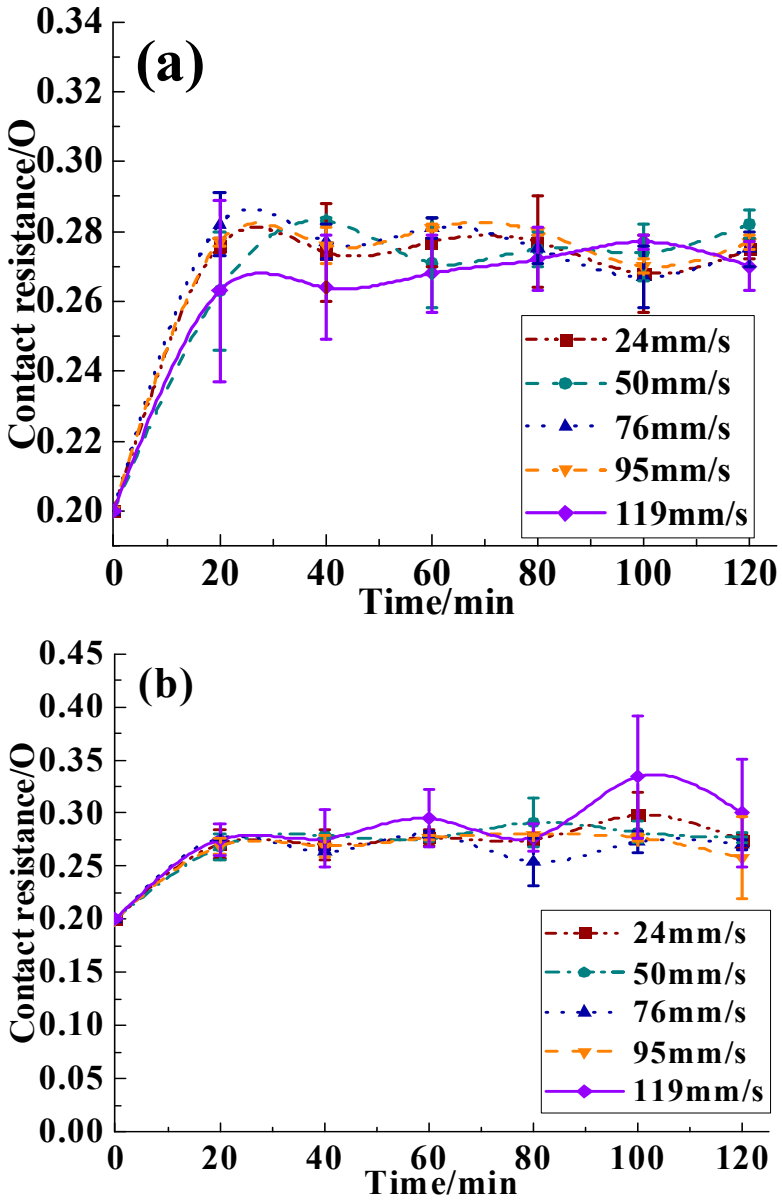

Figure 3. Contact resistance of OLTC couple at different sliding speeds in (**a**) air and (**b**) insulating oil.

3.1.2. Variations of Contact Resistance at Different Sliding Speeds

The testing results also reveal the dependence of the contact resistance on the sliding speed. Specifically, for the first three speeds (i.e., 24 mm/s, 50 mm/s, 76 mm/s), the contact

resistance is the same after 120 min sliding in both media, which is within the range of 0.27 Ω to 0.282 Ω. The contact resistance increases by an average of 39.67% in the air and 36.83% in the insulating oil after 120 min sliding. When the sliding speed is 95 mm/s, the contact resistance in the air and insulating oil increases by 38.5% and 29%, respectively. When the sliding speed further increases to 119 mm/s, the contact resistance in air and insulating oil increases by 35% and 50%, respectively. The increase in the contact resistance in insulating oil is much higher than that in air. In summary, the sliding speed impacts the contact resistance in insulating oil more than in air. Such impacts become more significant when the sliding speed increases.

3.2. Micro-Morphology Analysis of Contact Surface

To further analyze the impacts of the sliding speed on the tribological properties of the contact couple, the micro-morphology images of the contact surface after each test are shown in Figure 4, while the micro-morphological characteristics of the contact surface at different sliding speeds in air and insulating oil are summarized in Table 2.

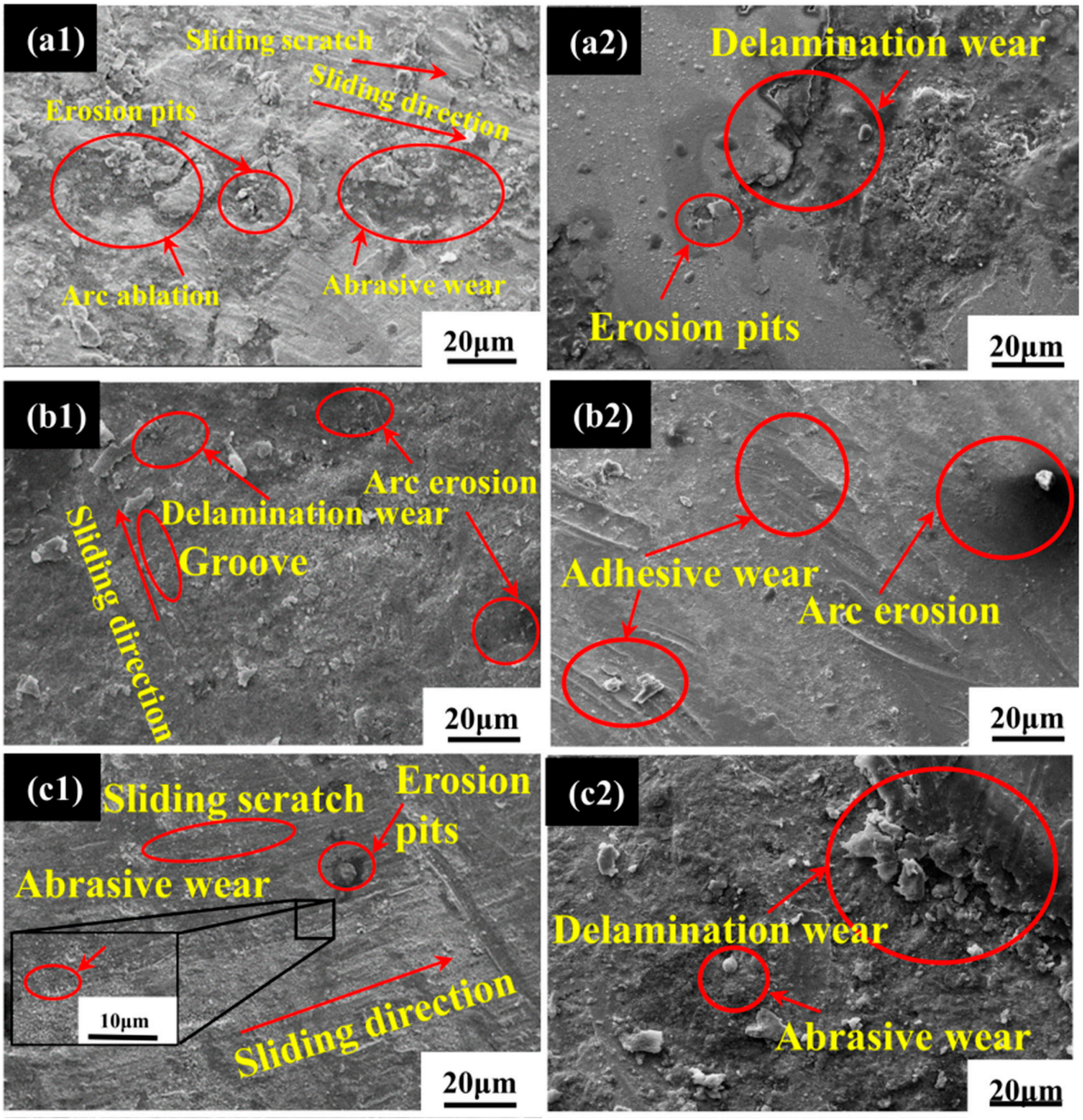

Figure 4. *Cont.*

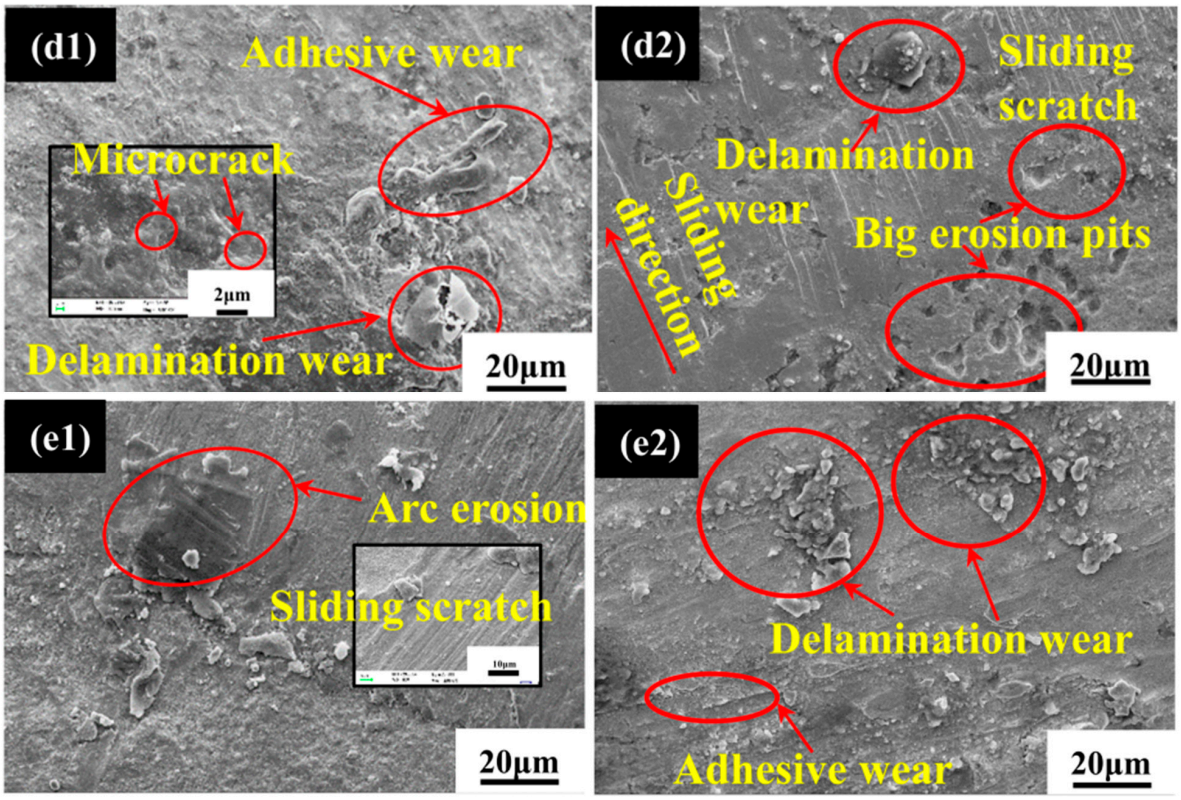

Figure 4. Micro-morphology of the contact surface after 120 min sliding in air (**a1**–**e1**) and insulating oil (**a2**–**e2**) at the speed of (**a1**,**a2**) 24 mm/s, (**b1**,**b2**) 50 mm/s, (**c1**,**c2**) 76 mm/s, (**d1**,**d2**) 95 mm/s and (**e1**,**e2**) 119 mm/s.

Table 2. Micro-morphology characteristics at different sliding speeds in air and insulating oil.

Insulating Dielectrics	Sliding Speed (mm/s)				
	24	**50**	**76**	**95**	**119**
Air	Scratches, abrasive wear and slight arc erosion	Scratches, grooves, and arc erosion	Erosion pits, abrasive wear	Adhesive wear, micro-cracks and delamination wear	Arc erosion
Oil	Erosion pit and delamination wear	Arc erosion and adhesive wear	Abrasive wear and delamination wear	Scratches, delamination wear and large erosion pits	Adhesive wear and delamination wear

Figure 4 shows that sliding speed significantly impacts the micro-morphology of the contact surface. For example, when the sliding speed is 24 mm/s, scratches, abrasive wear and slight arc erosion traces are observed on the contact surface in the air, while erosion pits and peeling wear are observed in the insulating oil. When the sliding speed increases to 50 mm/s, scratches, grooves and arc erosion traces appear on the contact surface in the air, while arc erosion and adhesive wear are observed in the insulating oil. At the sliding speed of 76 mm/s, scratches, erosion pits and abrasive wear traces are exhibited on the contact surface along the sliding direction in the air. In contrast, delamination and abrasive wear can be observed in the insulating oil. At the highest sliding speed (i.e., 119 mm/s), the contact surface experiences scratch and arc erosion in the air and adhesion wear and delamination wear in the insulating oil.

3.3. Element Analysis of Contact Surface

3.3.1. Element Analysis of the Contact Surface in Air

To reveal whether the chemical oxidation occurs on the contact surface during the electrical sliding and the associated oxidation mechanism, the EDS energy spectrum analysis was performed on the contact surface specimens collected at different speeds in two testing scenarios. The XPS energy spectrum analysis was also conducted on the contact surface after 120 min sliding at 119 mm/s. The major function of the EDS energy spectrum is to determine the chemical elements on the contact surface. The XPS energy spectrum is responsible for analyzing the chemical valence of the material surface. After peak fitting, the spectrum can be divided into two peaks: metal peak (Cu^0) with 932.3 eV and CuO peak (Cu^{2+}) with 933.9 eV [14]. Figure 5 shows the EDS energy spectrum of the contact surface in air. It shows that the ratio between oxygen and copper elements at each sliding speed is 0.068 (24 mm/s), 0.25 (50 mm/s), 0.308 (76 mm/s), 0.049 (95 mm/s) and 0.087 (119 mm/s). This ratio significantly increases when the sliding speed is 50 mm/s and 76 mm/s, indicating that more copper atoms participate in forming copper oxide and other substances at these speeds.

According to previous research, the ratio of O:Cu atoms can reflect the degree of contact surface fatigue phenomenon to a certain extent [15]. When the number ratio of atoms is relatively low, it indicates that there may be a fatigue peeling phenomenon on the contact surface. At this time, the surface fatigue degree is substantial. Combined with the change in O:Cu atomic ratio in air, the O:Cu atomic ratio of 95 mm/s and 119 mm/s at high speed is small or close to the initial atomic ratio. The fatigue peeling phenomenon is relatively apparent at high sliding speeds. Through the cross-validation from the XPS energy spectrum at 119 mm/s in Figure 6 and Table 3, it appears that CuO is formed on the contact surface. Based on the low conductivity of copper oxide and sulfide, the area where the fatigue peeling position enters and leaves during the sliding process will change the friction pair's contact performance. The non-uniform oxidation of the surface at high sliding speed will lead to the fluctuation of the conductivity of the contact area, thus causing the fluctuation of the contact resistance. That is, there is a specific relationship between the damage to the contact surface and the contact resistance change.

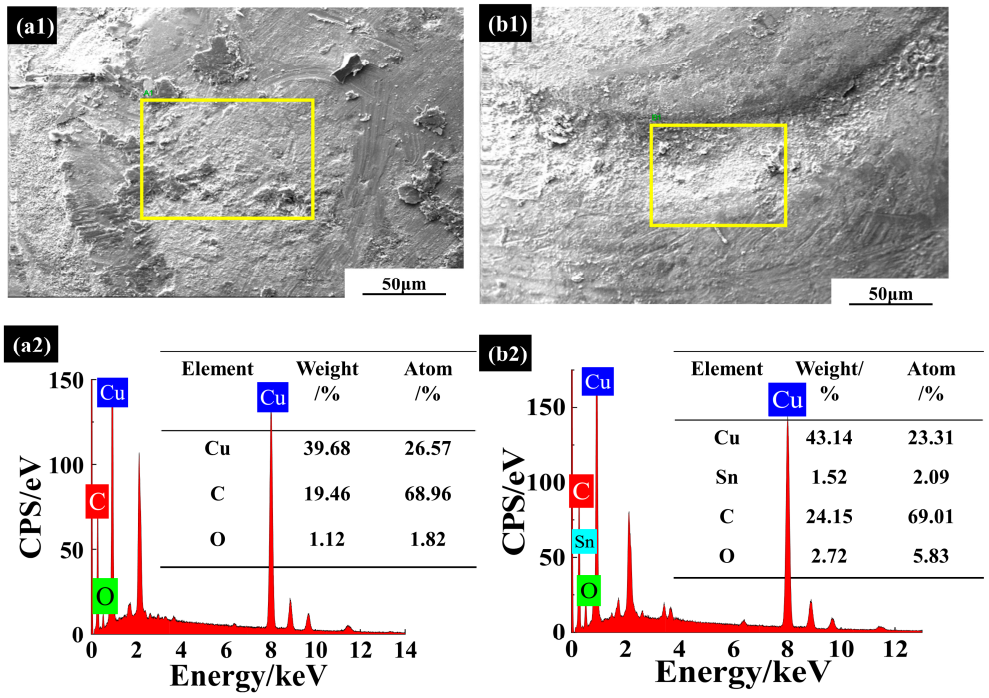

Figure 5. *Cont.*

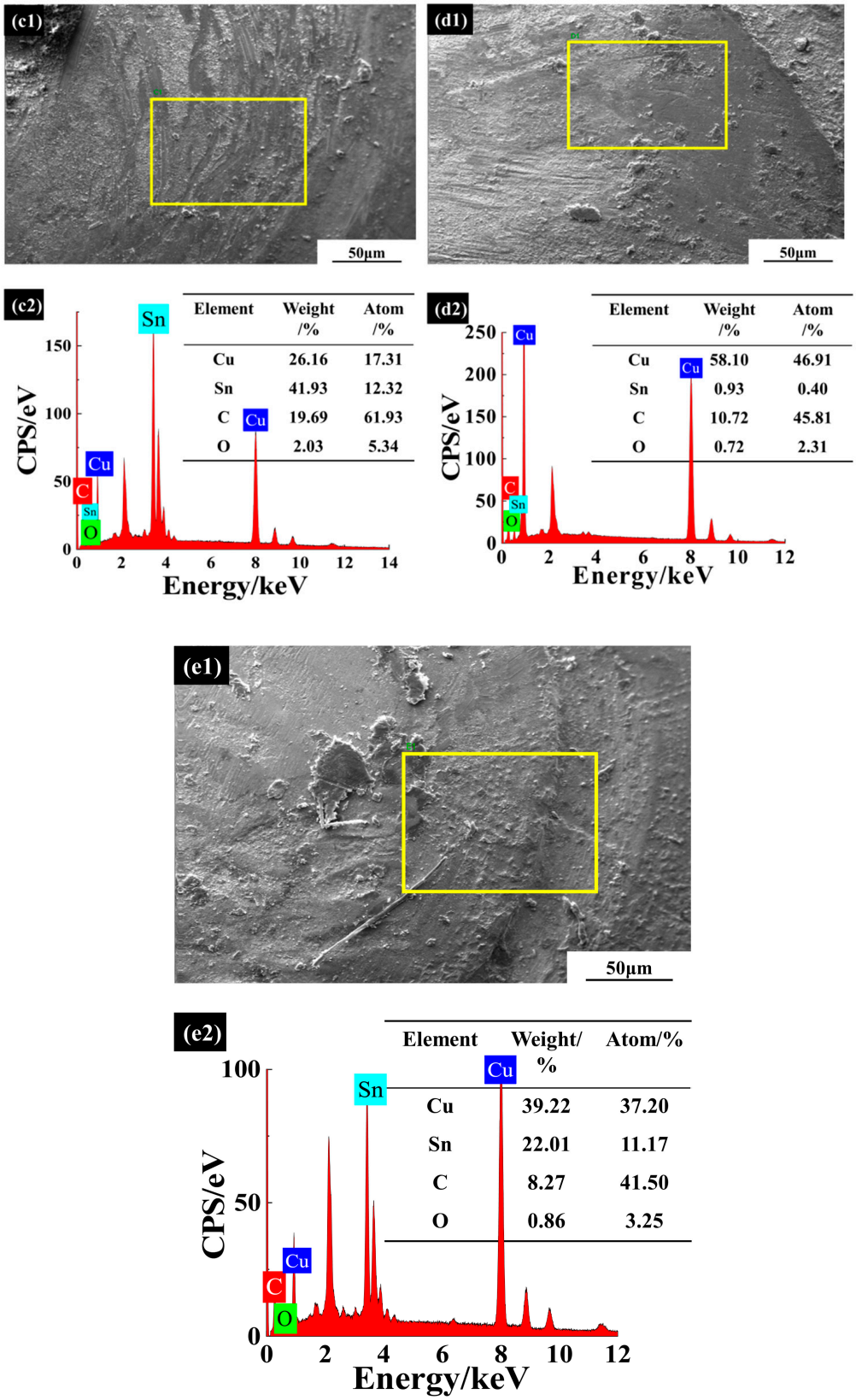

Figure 5. Micro-morphology of the contact surface in air (**a1**–**e1**) and corresponding EDS energy spectrum of magnified yellow areas (**a2**–**e2**) at the sliding speeds of (**a1**,**a2**) 24 mm/s, (**b1**,**b2**) 50 mm/s, (**c1**,**c2**) 76 mm/s, (**d1**,**d2**) 95 mm/s and (**e1**,**e2**) 119 mm/s. (The part circled by the yellow box is the analysis area of EDS energy spectrum).

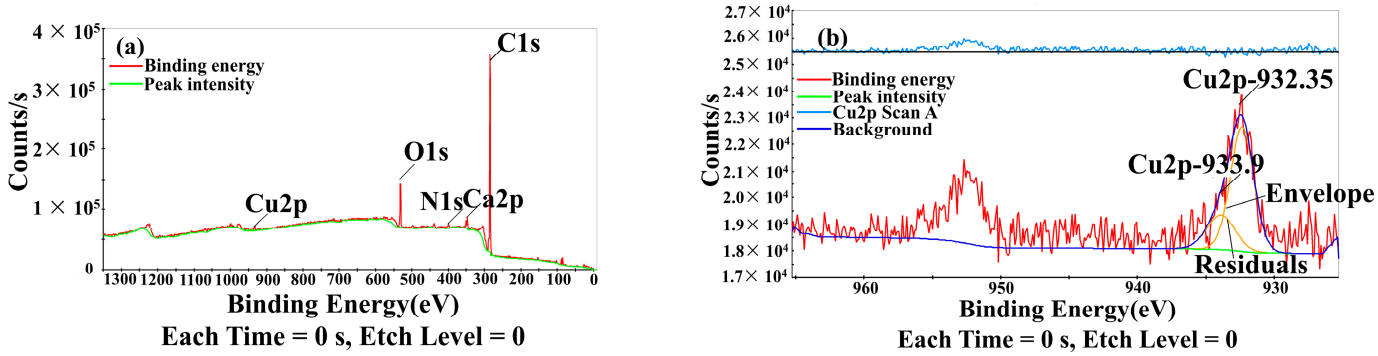

Figure 6. XPS energy spectrum of the contact surface in the air after 120 min sliding at the speed of 119 mm/s. (**a**) Overall test results, (**b**) Cu peak spectrum.

Table 3. Chemical valence and atomic percentage of peak elements in the air at the sliding speed of 119 mm/s.

Element	O1s	S2p	C1s	Cu2p
Atom/%	6.32	1.53	90.25	1.89

3.3.2. Element Analysis of the Contact Surface in Insulating Oil

Figure 7 shows the EDS energy spectrum of the contact surface in the insulating oil. The ratio between the oxygen and copper elements at each sliding speed is calculated as 1.411 (24 mm/s), 0.328 (50 mm/s), 0.376 (76 mm/s), 0.27 (95 mm/s) and 1.174 (119 mm/s). Compared with the results in air, the ratio between the oxygen and copper elements in insulating oil is higher, especially when the sliding speed is 24 mm/s and 119 mm/s. This indicates that copper atoms are more actively involved in forming the oxide film in the insulating oil, and the chemical reaction becomes more intensive. It is worth noting that the EDS energy spectrum in the insulating oil shows the sulfur elements which are not discovered in the air. Combining the XPS energy spectrum results in insulating oil at 119 mm/s (as shown in Figure 8) and the chemical valence and atomic percentage of peak elements in insulating oil at 119 mm/s (Table 4), the presence of sulfur ions is also confirmed. It is inferred that the contact surface may contain sulfur elements, sulfur-containing hydrocarbons or other forms of sulfides. By integrating the results of the energy spectrum of copper at the sliding speed of 119 mm/s (Figure 8c), it implies that copper-related compounds are formed on the contact surface in the insulating oil during the electrical sliding [16].

Table 4. Chemical valence and atomic percentage of peak elements in oil at the sliding speed of 119 mm/s.

Element	Cu2p	O1s	S2p	C1s
Atom/%	3.32	4.87	3.06	88.75

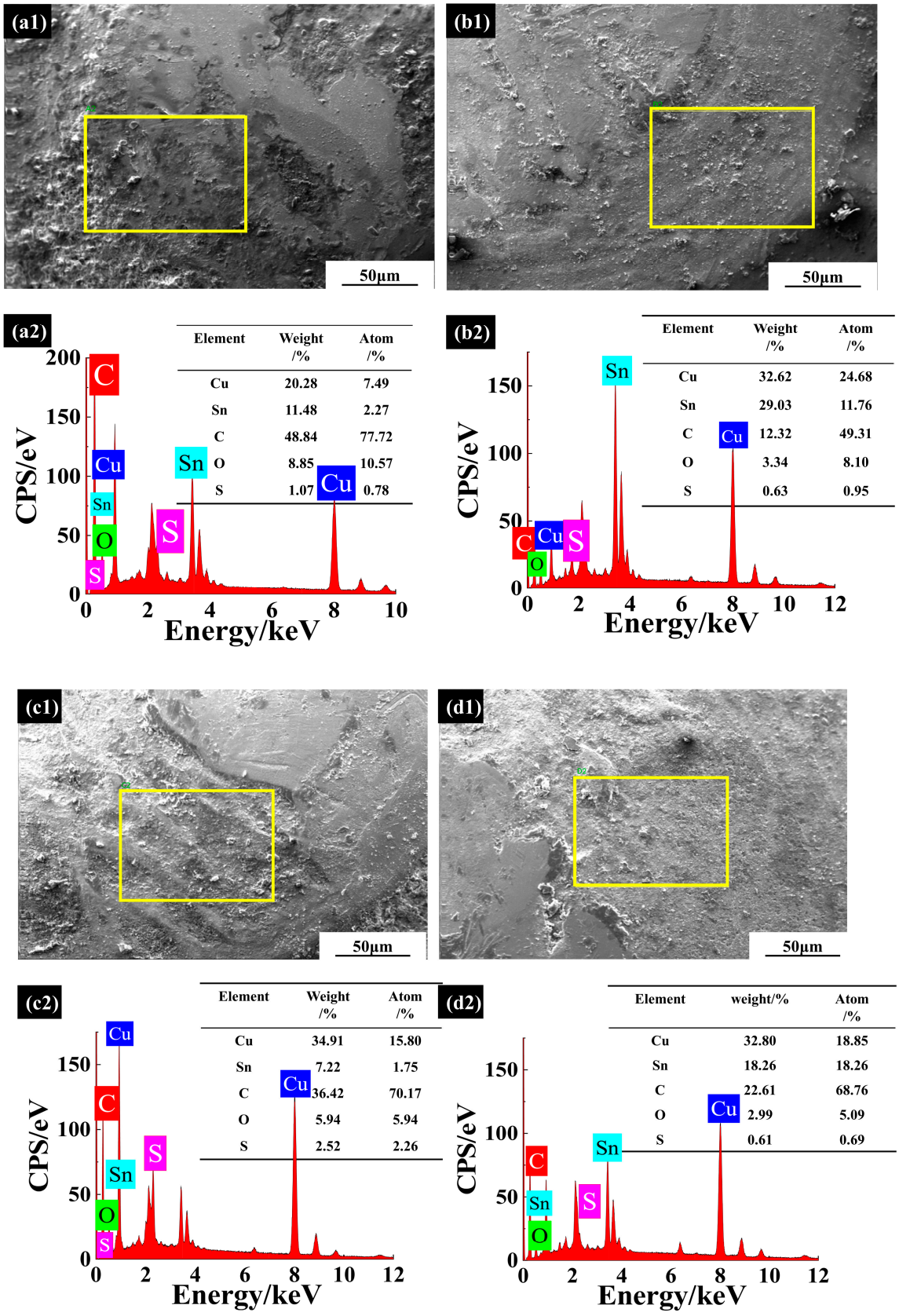

Figure 7. *Cont.*

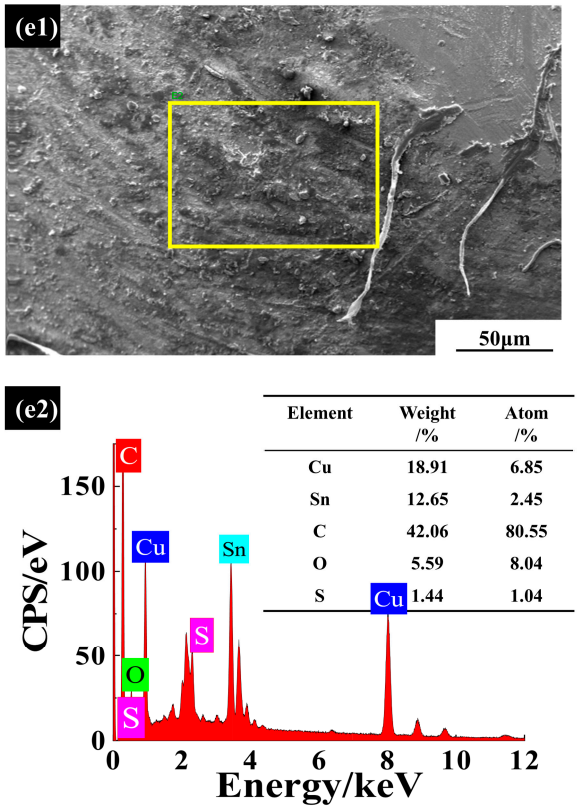

Figure 7. Micro-morphology of the contact surface in oil (**a1**–**e1**) and the corresponding EDS energy spectrum of magnified yellow areas (**a2**–**e2**) at the sliding speeds of (**a1**,**a2**) 24 mm/s, (**b1**,**b2**) 50 mm/s, (**c1**,**c2**) 76 mm/s, (**d1**,**d2**) 95 mm/s and (**e1**,**e2**) 119 mm/s. (The part circled by the yellow box is the analysis area of EDS energy spectrum).

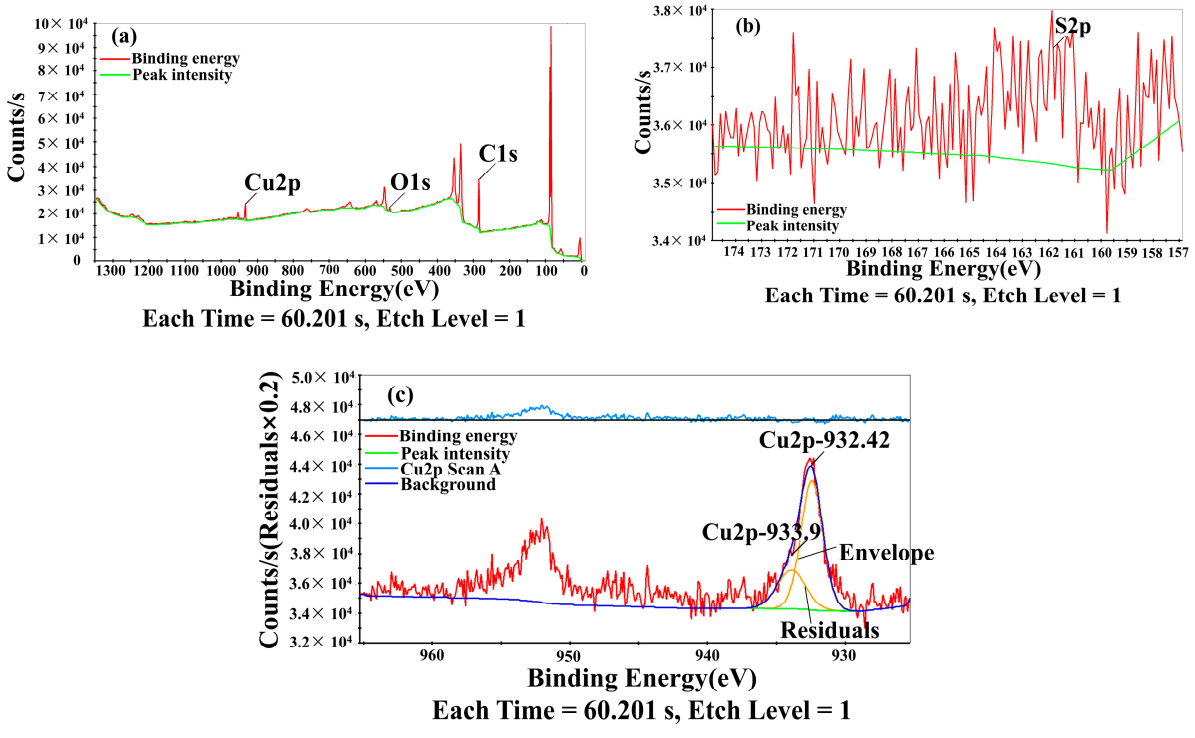

Figure 8. XPS energy spectrum of the contact surface in insulating oil after 120 min sliding at the speed of 119 mm/s. (**a**) Overall test results, (**b**) energy spectrum of sulfur element, (**c**) Cu peak spectrum.

4. Degradation Mechanism of Contact Couple

Based on the above experimental results, this section discusses the possible mechanism of the degradation of the contact couple during electrical sliding in the air and the insulating oil environment with focuses on three aspects: (1) micro-morphology mechanism analysis, (2) element content analysis and (3) microscopic contact resistance variation.

4.1. Micro-Morphology Analysis

4.1.1. Influence of Force on Micro-Morphology

During the electrical sliding, the contact surface experiences specific shear and normal stress, significantly influencing its deformation and degradation, given that a certain amount of water vapor may concentrate on the contact surface during the experiment. As a special liquid, insulating oil will cause the contact couple to be affected by the liquid in the sliding process. Therefore, the following forces may be exhibited during the movement of the contact:

- Adhesion effect between the static and moving contacts. In the process of electrical sliding, a large amount of energy will be transmitted through the contact surface, which means the current generates a large amount of Joule heat. Such current will produce an electromagnetic force that promotes adhesion between the contact surfaces. This adhesion may exist in both air and insulating oil medium.
- Meniscus force between the insulating oil (liquid) and the contact couple (solid) [17]. Due to the presence of the insulating oil between the static and moving contacts, meniscus force will be generated. Since the insulating oil also has a specific capillary effect, this will, in turn, further enhance the meniscus force. The meniscus force along the normal direction of the contact surface plays a dominant role in determining the degradation of the contact surface [18].
- Adhesion effect of the insulating oil itself. Since the kinematic viscosity of the insulating oil in the experiment is 9.395 (at 40 °C), which is much higher than that of air, an adhesive force will be formed along the tangential direction of the contact surface during the sliding, which will eventually increase the tangential force. With the increase in sliding speed, the movement of the moving contact in the insulating oil will also be subject to liquid resistance.
- Meniscus force induced by the electric field. It has been reported that the electric field would enhance the generation of meniscus force in the water [19]. Therefore, it is assumed that the electric field will induce meniscus force in the insulating oil.
- Gravity force and thermal buoyancy. During the sliding process, the temperature of the contact surface increases, and such an increase becomes more prominent when the sliding speed is higher [20]. Therefore, thermal buoyancy may have a specific impact on the contact surface, requiring further investigation.
- Arc force. The last force influencing the contact surface is the arc force which is generated during the electrical sliding. Specifically, the arc flow will increase at high sliding speeds, which leads to increased arc pressure applied on the contact surface [21]. It is assumed that the force acts in the direction of contact separation. The arcing activity under oil is higher than that under air because oil's insulating capability is higher than air. Compared with air, the meniscus force generated by the insulating oil is much more vital. Therefore, the following section mainly focuses on the force analysis of the contact surface in the insulating oil, which is shown in Figure 9. Table 5 shows the explanation of the terms in Figure 9 and the meaning of some parameters in the following formula.

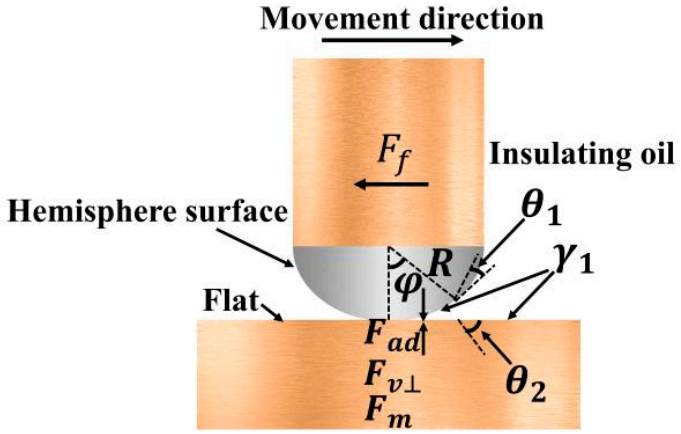

Figure 9. Force analysis diagram of contact couple in insulating oil.

Table 5. Explanation of terms in Figure 9 and meanings of some parameters in the following formula.

Parameters	Meaning
θ	Angle between insulating oil and copper contact surface
φ	The half-angle of the contact area
F_{ad}	Adhesive force: A type of molecular force that represents the adhesion between the insulating oil and the contact surface, including the adhesion force caused by the meniscus force and the sliding speed
F_m	Adhesive force dominated by the meniscus force
$F_{v\perp}$	Adhesive force dominated by the sliding speed
R	The radius of the moving contact tip
γ_1	The surface energy of the insulating oil medium; surface energy is a measure of the breaking of chemical bonds between molecules when creating the surface of a substance
μ	The dynamic viscosity coefficient
v	Sliding speed
dv/dx	The velocity gradient
K_1	Constant determined by different liquids
F_f	Resistance against the direction of motion

When there is a specific contact angle θ between the insulating oil and the copper contact surface, the insulating oil will concentrate or penetrate small holes or cracks on the copper contact surface during the sliding, which leads to the formation of annular droplets in the contact area. The insulating oil acts as a liquid film, which will significantly increase the adhesion of the copper contact surface. In this case, the adhesive force caused by the meniscus force mainly consists of two components: one component is related to the meniscus force caused by the liquid surface tension, and the other component is mainly determined by the sliding speed, as expressed in the Formula (1).

$$F_{ad} = F_m + F_{v\perp} \tag{1}$$

where F_{ad} is the adhesive force, F_m is the adhesive force dominated by the meniscus force and $F_{v\perp}$ is the adhesive force dominated by the sliding speed.

In Figure 9, the angle $\theta_1 = \theta_2$, φ is the half-angle of the contact area, which is the angle between the insulating oil plane and the center of the moving contact. The angle φ will increase as the moving contact is gradually immersed in the insulating oil. In this case, the meniscus force can be expressed as Formula (2):

$$F_m = 4\pi R\gamma_1 K_1 \cos\theta_1 + 2\pi R \sin\varphi \sin(\varphi + \theta_2) \tag{2}$$

where R is the radius of the moving contact tip, γ_1 is the surface energy of the insulating oil medium [17] and K_1 is a constant determined by different liquids.

According to Newton's law of viscosity, the viscous force can be expressed as Formula (3):

$$F_{v\perp} = \mu \frac{\mathrm{d}v}{\mathrm{d}x} \tag{3}$$

where μ is the dynamic viscosity coefficient, v is sliding speed and $\mathrm{d}v/\mathrm{d}x$ is the velocity gradient.

In the insulating oil, the adhesive force can be expressed as Formula (4):

$$F_{ad} = 4\pi R\gamma_1 K_1 \cos\theta_1 + 2\pi R \sin\varphi \sin(\varphi + \theta_2) + \mu \frac{\mathrm{d}v}{\mathrm{d}x} \tag{4}$$

From the above analysis, it is clear that when the whole contact surface begins to be immersed in the insulating oil, the value of φ becomes large, which increases F_m. When the contact surface is fully immersed in the insulating oil, the value of φ remains constant.

4.1.2. Influence of Arcing on the Micro-Morphology

The micro-morphology of the contact surface is also influenced by the arcing during the electrical sliding. Tables 6 and 7 summarize the breakdown voltage amplitude, average value of breakdown voltage, arc discharge energy, arc discharge energy amplitude and discharge frequency in air and insulating oil at different speeds after 120 min sliding. It can be seen from Table 6 that the average value of breakdown voltage in the air gradually decreases when the sliding speed increases from 24 mm/s to 95 mm/s. However, the average breakdown voltage value increases again at the speed of 119 mm/s. When the sliding speed is 24 mm/s, 50 mm/s and 76 mm/s, the amplitude of the breakdown voltage remains stable and varies between 0.512 V and 0.584 V. However, when the sliding speed is 95 mm/s, the amplitude of the breakdown voltage rises significantly to 3.62 V. Based on the micro-morphology measurements of SEM, the deterioration of the contact surface becomes more severe at the sliding speed of 95 mm/s. When the sliding speed is 119 mm/s, the amplitude of the breakdown voltage also becomes higher. The micro-morphology shows that the arc erosion area at this speed is more significant than that at the first three speeds. Based on the above analysis, it is clear that a speed threshold exists between 95 mm/s and 119 mm/s. If the sliding speed exceeds this threshold, the average value and amplitude of breakdown voltage will rise significantly, and the bombardment of the arc on the contact surface will be enhanced, which results in severe deterioration of the contact surface.

Table 6. Electrical breakdown of the contact couple in the air after 120 min sliding.

Speed (mm/s)	Breakdown Voltage Amplitude (V)	Average Breakdown Voltage (V)	Arc Discharge Energy (J)	Arc Discharge Energy Amplitude (J)	Breakdown Frequency
24	0.579	0.055	0.088	0.366	281
50	0.512	0.032	0.034	0.346	171
76	0.584	0.026	0.204	0.388	63
95	3.620	0.016	0.015	0.372	49
119	1.181	0.075	0.013	0.381	98

Table 7. Electrical breakdown of the contact couple in insulating oil after 120 min sliding.

Speed (mm/s)	Breakdown Voltage Amplitude (V)	Average Breakdown Voltage (V)	Arc Discharge Energy (J)	Arc Discharge Energy Amplitude (J)	Breakdown Frequency
24	4.137	0.051	0.004	0.300	120
50	3.200	0.015	0.001	0.230	29
76	3.926	0.006	0.007	0.305	46
95	3.185	0.097	0.002	0.205	25
119	0.940	0.059	0.003	0.240	82

Table 7 shows the breakdown voltage measurements in the insulating oil. It is found that the average value of breakdown voltage shows a decreasing trend when the sliding speed increases from 24 mm/s to 76 mm/s. Afterward, it rises to 0.097 V at 95 mm/s and decreases again at 119 mm/s. The amplitude of the breakdown voltage remains relatively stable at the first four speeds. It is also found that there is a certain degree of delamination wear and arc erosion at the first four speeds; when the sliding speed is 95 mm/s, the distribution of the erosion pits becomes the densest. It is speculated that because the average value of the breakdown voltage is the largest and the amplitude of the breakdown voltage is large, the bombardment and ablation of the arc on the surface will reach the maximum, which will lead to the most severe surface deterioration at the speed of 95 mm/s. In the separating process of the moving and static contact, the arc air velocity gradually increases, and the arc pressure in the contact area increases with the speed increase. It is speculated that the arc force will also cause certain erosion on the contact surface [21]. When the sliding speed is higher, the larger the arc current is, the larger the high-temperature area of the arc is, and the more serious the ablation degree of the material is [20]. At the same time, it is speculated that there is also a critical speed in the insulating oil such that the average breakdown voltage reaches the maximum at about 95 mm/s, and the erosion effect of the arc on the contact surface is the most obvious. Limited by the testing scenarios, this critical speed needs further refinement in future work.

4.2. Analysis of Surface Compound Formation Mechanisms

4.2.1. Formation of Copper Oxide in Air

From the previous EDS analysis and XPS analysis of the contact surface in the air, the valence of the elements and corresponding elements on the contact surface can be identified. The oxidation formed during the electrical sliding is related to tribochemical and electrochemical oxidation. Through the above tests, it can be inferred that there may be an oxide film composed of copper oxide and other substances on the contact surface. Figure 10a illustrates the formation of copper oxide in the air. The possible reaction mechanism is as follows: Due to the vapor in the air, the copper surface will adsorb the vapor and generate hydroxyl on its surface. The hydroxyl generated on the surface can promote the adsorption of vapor in the air. The copper surface can be chemically modified by hydroxylation to form hydroxyl termination in the contact area of the contact surface [22]. Excited by the action of internal energy such as friction energy, Joule heat and arc heat, the dehydration reaction may form a copper–oxygen–copper bond [23]. During the sliding process, such a bond is repeatedly stretched so mechanical energy can be stored. Due to the absorption of the vapor, these high-energy bonds are destroyed by the adsorbed water through a hydrolysis reaction, resulting in a copper oxide film. Due to the copper oxide's low conductivity, the oxide's formation leads to an increase in contact resistance. Due to the limited water adsorbed during the sliding process, the formation of the copper oxide film is insignificant, so the contact resistance does not fluctuate in an extensive range at each sliding speed.

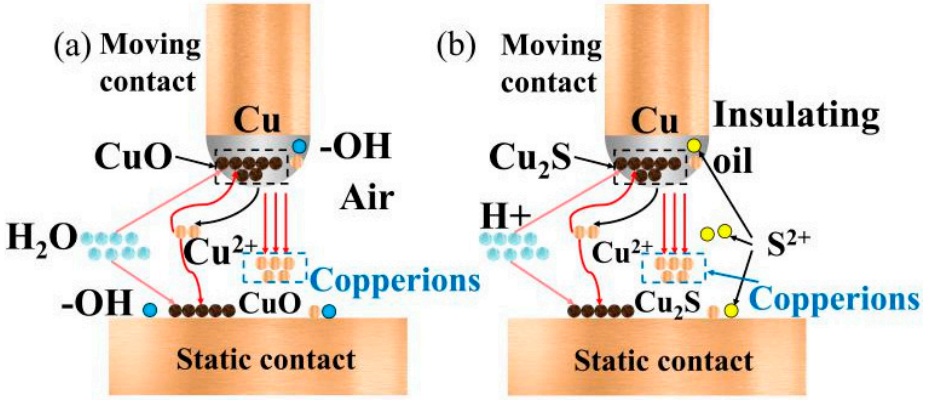

Figure 10. Formation mechanisms of (**a**) copper oxide in air and (**b**) cuprous sulfide in insulating oil.

4.2.2. Formation of Cuprous Sulfide in Insulating Oil

From EDS analysis in Figure 7 and XPS analysis in Figure 8b, it is found that sulfur elements exist on the contact surface of the insulating oil and the valence state is divalent. It has been reported that disulfide is the most common corrosive sulfide [24]. Therefore, it is speculated that the highly active sulfide in the insulating oil may react with the copper contact to form copper sulfide or cuprous sulfide. Some copper sulfides or cuprous sulfide particles may be attached to the surface of the copper contact. The rest may form the abrasive particles as observed in the SEM image, resulting in abrasive wear. With the formation of abrasive particles and the movement of the contact, copper sulfide or cuprous sulfide will be deposited on the contact surface in the form of the surface film. Some copper sulfides or cuprous sulfide particles may migrate to the insulating oil medium, thus reducing the resistance of insulating oil and lowering the breakdown voltage. Copper sulfide or cuprous sulfide produced by sulfur corrosion can also be dissolved in insulating oil. Impurity bridges will be formed under the action of the electric field, which results in breakdown. At the same time, the dielectric loss of insulting oil will increase. It is speculated that this will increase the charging tendency of the insulating oil, resulting in a reduction in the breakdown voltage of the insulating oil. As indicated in Table 7, the increase in the amplitude and the average value of breakdown voltage in insulating oil may be related to the formation of copper sulfide or cuprous sulfide. When the insulating oil contains copper sulfide or cuprous sulfide impurities and flows with the movement of the contact couple, the charge separation ability at the interface between the insulating oil and the solid insulating material will be enhanced. Due to the influence of the electric field, velocity, gravity field and other factors, electrons and positive ions will obtain different velocities in different directions. This will lead to an ununiform distribution of electrons and positive ions, which finally causes the formation of space charges. The increasing sliding speed of the moving contact also increases the flow speed of the insulating oil containing copper sulfide or cuprous sulfide. This further increases the charge separation ability of the insulating oil around the contact surface and weakens the ability to release the free charge in the oil. Therefore, substantial local charges accumulate between the copper contacts and the surrounding oil flow. When this charge accumulates to a certain extent, a cloud-like DC electromotive force difference will be formed in the oil, resulting in breakdown flashover discharge.

As a semiconductor, copper sulfide or cuprous sulfide will affect the distribution of electric field between the moving and static contacts, which will, in turn, affect the generation of copper sulfide or cuprous sulfide. It is speculated that the presence of the electric field in the contact couple immersed in insulating oil will accelerate the corrosion of copper contacts by sulfur in insulating oil [25]. The fundamental principle of such corrosion is shown in Figure 10b.

The moving contact and static contact act like an electrolytic cell in insulating oil, which will form electrochemical corrosion between the copper rod and the copper plate. The moving contact acts as an anode, and the static contact acts as a cathode. After a specific time of sliding, the surfaces of the moving and static contacts will release some copper ions into the insulating oil and reduce the breakdown voltage of the insulating oil. At the same time, the presence of sulfide in the insulating oil will also promote the formation of copper sulfide or cuprous sulfide. Some copper sulfides or cuprous sulfide particles are deposited on the contact surface during sliding. According to the calculated contact resistance in insulating oil (Figure 3b), it is speculated that the deposition of copper sulfide or cuprous sulfide improves the volume resistivity and surface resistivity of the contact surface. The test results also show that copper sulfide or cuprous sulfide deposition may be relatively stable at the first three sliding speeds, and the contact resistance shows minimal changes. As the sliding speed further increases, inevitable fluctuations of contact resistance appear. It is speculated that the increase in the breakdown voltage will accelerate the formation of copper sulfide or cuprous sulfide and their deposit on the contact surface. Finally, this will

increase the resistance of the surface film. The reaction between active sulfide and copper in insulating oil will produce cuprous sulfide through the following reactions [26]:

$$4Cu + O_2 \rightarrow 2Cu_2O \quad (5)$$

$$Cu_2O + 2RSH \rightarrow 2CuSH + H_2O \quad (6)$$

$$2CuSH \rightarrow Cu_2S + RSR \quad (7)$$

Since the contact surface of the on-load tap changer under long-term operation may produce copper oxide or cuprous sulfide and other substances, the semi-conductivity of the above substances has an important impact on the dielectric property of insulating oil. The presence of cuprous sulfide and other substances will increase the conductivity of the insulating oil, which may increase the number of partial discharges near the contact, leading to an increase in the frequency of arc breakdown. Therefore, the insulating oil should be sampled regularly to determine the degree of contact deterioration and oxidation reaction by detecting the sulfide content in the insulating oil.

4.3. Macroscopic Contact Resistance Variation

4.3.1. Macroscopic Contact Resistance Variation in Air

According to the testing results in Figure 3a, the contact resistance in the air is relatively stable, and the mechanical wear and arc ablation on the contact surface is dominant. With the increase in the sliding speed, mechanical wear leads to plastic deformation of the micro-morphology of the contact surface. In contrast, arc ablation leads to flake fatigue wear, and arc ablation changes the contact surface. Tribochemical and electrochemical oxidation play a secondary role in the degradation of the contact surface. According to the EDS and XPS analysis, it is found that copper oxide and other substances are generated on the contact surface, which leads to the change of contact resistance. Due to limited water vapor in the air, the degree of the oxidation reaction is low, and the content of copper oxide is minimal.

4.3.2. Macroscopic Contact Resistance Variation in Insulating Oil

Based on the testing results in Figure 3b, the contact resistance in the insulating oil is relatively stable at the initial stage, and the contact resistance fluctuates wildly at high speed, especially at 119 mm/s. It is speculated that different types of mechanical action, arc ablation, chemical oxidation and electrochemical oxidation play a significant role in determining the contact resistance in the insulating oil. The mechanical action mainly involves meniscus force and pressure of insulating oil on the contact surface. The wear mechanism of the contact surface is mainly delamination wear and erosion pits. At the same time, arc ablation also accelerates the formation of erosion pits. When the sliding speed is 95 mm/s, the average value of breakdown voltage reaches the maximum, and the amplitude of breakdown voltage is also significant, indicating the bombardment and erosion of the arc on the contact surface reaches the maximum. Copper sulfide and cuprous sulfide are the main reasons for the increase in contact resistance. Especially when the sliding speed is 119 mm/s, the increase in the average and maximum breakdown voltage accelerates the deposition of copper sulfide and cuprous sulfide on the contact surface, which further increases the resistance of the surface film and makes the contact resistance increase significantly compared with other speeds.

5. Conclusions

This paper presents a comprehensive experiment to investigate the impacts of sliding speed on the degradation of the contact couple in an OLTC. Through SEM, EDS and XPS tests, combined with electrical characteristics such as contact resistance, the degradation mechanism of the contact surface at different sliding speeds is analyzed, and the mechanical and chemical oxidation reactions caused by insulating oil are discussed. The main conclusions are as follows:

- When the sliding speed increases from 24 mm/s to 119 mm/s, the average contact resistance in air and insulating oil medium increases by 39.67% and 36.83%, respectively. After 120 min of sliding, the initial contact resistance is 0.2 Ω, and the final average contact resistance is 0.276 Ω and 0.267 Ω, respectively. Compared with air, the contact resistance in insulating oil shows more significant fluctuation at high sliding speed and reaches 0.3 Ω at 119 mm/s.
- There are critical velocities in air and insulating oil, and different wear mechanisms appear before and after the critical velocities. The critical velocity in air is about 119 mm/s, and that in insulating oil is about 95 mm/s. Below this speed, mechanical wear plays a significant role in the deterioration of the contact surface. When the velocity exceeds this threshold, arc ablation and chemical oxidation are the main reasons for the deterioration of the contact surface.
- At different sliding speeds, tribological oxidation and electrochemical oxidation lead to the formation of the copper oxide film on the contact surface in the air. In the insulating oil, copper sulfide or cuprous sulfide appears on the contact surface. The oxide film increases the contact resistance, especially at high sliding speeds. The arcing also accelerates the generation of copper sulfide or cuprous sulfide on the contact surface, which increases the contact resistance at high sliding speeds. Therefore, it is necessary to determine the proper sliding speed of the contact couple in an OLTC to minimize mechanical wear and chemical oxidation in real-life operating conditions.

Author Contributions: Conceptualization, X.Y. and S.L.; methodology, Y.K.; software, H.D. and H.L.; validation, X.Y., S.L. and Y.K.; investigation, Z.L.; resources, Z.L.; data curation, X.Y.; writing—original draft preparation, X.Y.; writing—review and editing, S.L. and Y.C.; visualization, X.Y.; supervision, Y.K.; project administration, S.L.; funding acquisition, S.L. and Y.K. All authors have read and agreed to the published version of the manuscript.

Funding: This research was funded by the Gansu University Innovation Fund under contract No. 2021B-111, the Gansu Provincial Department of Education: Outstanding Graduate "Innovation Star" Project 2022CXZX-610 and Natural Science Foundation of Gansu Province under contract No. 21JR1RA255.

Institutional Review Board Statement: Not applicable.

Informed Consent Statement: Not applicable.

Data Availability Statement: Not applicable.

Conflicts of Interest: The authors declare no conflict of interest.

References

1. Allard, L.; Lorin, P.; Foata, M. Vibro-acoustic diagnostic: Contributing to an optimized on-load tap changer (OLTC) maintenance strategy. *Water Energy Int.* **2011**, *68*, 1–8.
2. CIGRE Brochure. Transformer reliability survey. *CIGRE Task Force* **2015**, *642*, 94–102.
3. Ma, Y.; Wang, S.; Wang, T.; Xu, J.; Wu, P.; Shi, Q.; Wu, Y. On load tap changer fault diagnosis method based on drive motor current and vibration signal. *High Volt. Appar.* **2022**, *58*, 202–210.
4. Fan, J.; Wang, F.; Zheng, Y. Mechanical condition monitoring of on- load tap changer based on recurrence quantification analysis. *High Volt. Appar.* **2019**, *55*, 197–203.
5. Zhang, X.; Zhang, K.; Kang, X.; Zhang, L. Friction maps and wear maps of Ag/MoS2/WS2 nanocomposite with different sliding speed and normal force. *Tribol. Int.* **2021**, *164*, 12. [CrossRef]
6. Namus, R.; Nutter, J.; Qi, J. Sliding speed influence on the tribo-corrosion behaviour of Ti6Al4V alloy in simulated body fluid. *Tribol. Int.* **2021**, *3*, 107023. [CrossRef]
7. Chen, T.; Song, C.; Zhang, Y. Current-carrying contact character and wear behavior of an elastic ring at different rolling speeds. *Eng. Fail. Anal.* **2022**, *131*, 1–10. [CrossRef]
8. Xie, X.; Zhang, L.; Xiao, J. Sliding electrical contact behavior of AuAgCu brush on Au plating. *Trans. Nonferrous Met. Soc. China* **2015**, *25*, 3029–3036. [CrossRef]
9. Noguchi, S. Turn-to-Turn Contact Resistance Measurement of No-Insulation REBCO Pancake Coil: External Field Dependence. *IEEE trans. Appl. Supercond.* **2021**, *31*, 4602105. [CrossRef]

10. Fukuyama, Y.; Sakamoto, N.; Kondo, T. Study of Contact Resistance in Connectors with Physical Simulation Using Nanofabrication. *IEEE Trans. Instrum. Meas.* **2017**, *66*, 1248–1253. [CrossRef]
11. Cheng, T.; Gao, W.; Zhao, D. Method to improve the repeatability of dynamic contact resistance measurement test results for high-voltage circuit breakers. *IET Sci. Meas. Technol.* **2019**, *13*, 544–552. [CrossRef]
12. Dutta, S.; Vikram, G.; Bobji, M.; Mohan, S. Table top experimental setup for electrical contact resistance measurement during indentation. *Measurement* **2019**, *152*, 107286. [CrossRef]
13. Popov, V.L. *Principles and Applications of Contact Mechanics and Tribology*, 2nd ed.; Tsinghua University Press: Beijing, China, 2019.
14. Zhang, Z.; Sun, L.; Wu, Z.; Liu, Y.; Li, S. Facile hydrothermal synthesis of CuO-Cu_2O/GO nanocomposites for the photocatalytic degradation of organic dye and tetracycline pollutants. *New J. Chem.* **2020**, *44*, 6420–6427. [CrossRef]
15. Sun, Y.; Song, C.; Li, J.; Zhang, Y.; Zhang, Y. Effect of rotating speed on rolling current carrying friction damage of pure copper in water environment. *Tribol* **2021**, *41*, 365–372.
16. Heide, P.V. *X-ray Photoelectron Spectrosco*; Wiley: Hoboken, NJ, USA, 2011.
17. Birleanu, C.; Pustan, M.; Rusu, F.; Dudescu, C.; Muller, R.; Baracu, A. Relative humidity effect on pull-off forces in MEMS flexible structures measured by AFM. In *2017 Symposium on Design, Test, Integration and Packaging of MEMS/MOEMS (DTIP)*; IEEE: Piscataway, NJ, USA, 2017; pp. 1–8.
18. Zamora, R.; Sanchez, C.; Freire, F. Influence of capillary condensation of water in nanoscale friction. *Phys. Status Solidi* **2010**, *201*, 850–856. [CrossRef]
19. Yan, L.; Jing, W.; Liang, X.; Liu, Y. Adhesion force measurement of electrical insulating materials by atomic force microscopy. In Proceedings of the 2012 Power Engineering and Automation Conference, Wuhan, China, 18–20 September 2012; pp. 1–5.
20. Gao, G.; Xu, P.; Wei, W. Modeling and analysis of magnetic fluid in descending arc under load conditions. *High Volt. Eng.* **2019**, *45*, 3916–3923.
21. Wu, Y.; Yang, Z.; Gao, G. Thermal ablation process of electrical contact materials under arc action. *High Volt. Eng.* **2019**, *45*, 2276–2283.
22. Shao, Y.; Jacobs, T.; Jiang, Y. A multi-bond model of single-asperity tribochemical wear at the nano-scale. *ACS Appl. Mater. Inter.* **2017**, *9*, 35333–35340. [CrossRef]
23. Dhayal, Y.; Chandel, C.; Gupta, K. The influence of hydroxyl volatile organic compounds on the oxidation of aqueous sulfur dioxide by oxygen. *Environ. Sci. Pollut. Res.* **2014**, *21*, 7805. [CrossRef]
24. Cong, H.; Zhang, M.; Li, Q. Study on Sulfide distribution in the operating oil of power transformers and its effect on the oil quality. *Appl. Sci.* **2018**, *8*, 1577. [CrossRef]
25. Yang, L.; Gao, S.; Deng, B. Corrosion mechanisms for electrical fields leading to the acceleration of copper sulfide deposition on insulation windings. *Ind. Eng. Chem. Res.* **2017**, *56*, 9124–9134. [CrossRef]
26. Hajek, J.; Bennstam, G.; Dahlund, M. Quality of oil makes the difference, ABB discovers the solution to transformer breakdown. *ABB Rev.* **2004**, *3*, 61–63.